Inorganic Chemistry

Article

pubs.acs.org/IC

# Synthesis, Crystal Structures, and Luminescence Properties of Carboxylate Based Rare-Earth Coordination Polymers

Roel Decadt,[†] Kristof Van Hecke,[†] Diederik Depla,[‡] Karen Leus,[†] David Weinberger,[†] Isabel Van Driessche,[†] Pascal Van Der Voort,[†] and Rik Van Deun*[,†]

[†]Department of Inorganic and Physical Chemistry, Ghent University, Krijgslaan 281, Building S3, 9000 Gent, Belgium

[‡]Department of Solid State Sciences, Ghent University, Krijgslaan 281, Building S1, 9000 Gent, Belgium

Supporting Information

**ABSTRACT:** Rare-earth coordination polymers or lanthanide–organic frameworks with hitherto unreported crystal structures have been obtained on the basis of the "light" lanthanides Pr, Nd, Sm, and Eu in combination with terephthalic acid and using a slightly altered literature synthesis procedure. Rietveld refinement has shown that powder XRD patterns of such compounds are largely dominated by the positions of the heavy elements, pointing to isostructural networks for all four terephthalate-based materials. An in-depth luminescence study has been performed on the reported MOFs, showing rare praseodymium and samarium emission in the visible spectrum, aside from the strong europium luminescence and the near-infrared emission from both a terephthalate and 2,5-pyridinedicarboxylate based neodymium-MOF.

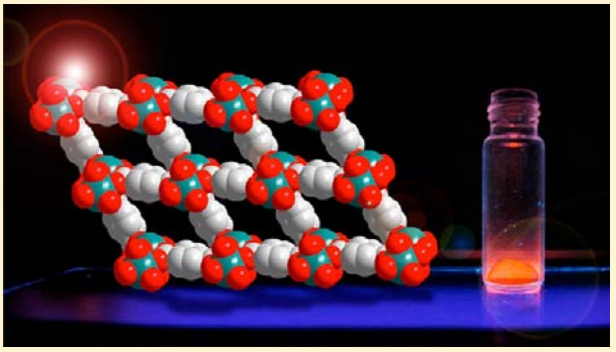

## INTRODUCTION

The past decade has seen an exponential growth of reports dealing with metal–organic frameworks (MOFs) or porous coordination polymers, which are being studied for their possible application in catalysis, gas separation, gas storage, ion exchange, luminescence, magnetism, etc.[1−14] Lanthanide–organic frameworks in particular are promising materials because of the intrinsic physical properties of the trivalent lanthanide ions, such as color-pure luminescence, large paramagnetism, and the fact that the electrostatic nature of their coordination chemistry allows a large variety of symmetries and structural patterns to be obtained, whereas the well-defined tetrahedral or octahedral coordination patterns of most of the transition metal ions limit this variety to a certain extent.[15−17]

Even though the symmetry of a transition metal coordination sphere limits the possible structural patterns that can be obtained in transition metal–organic frameworks, at least this symmetry could ideally allow the prediction of the main structural features of the resulting MOF. This is not at all the case for lanthanide–organic frameworks. As a result, the understanding of the mechanisms that lead from lanthanide salt and linker molecules to the resulting lanthanide clusters is still nowhere near complete. In this Article, we show that the cationic radius of the lanthanide, in combination with slight alterations to literature procedures, can lead to materials that are structurally different than the ones reported in the literature.

By far the most widely studied lanthanide–organic frameworks are based on linker molecules that contain carboxylate groups as the coordinating units, among which 1,4-benzenedicarboxylate (also known as terephthalate) is most likely the most popular one. In this Article, we extend the family of terephthalate-based lanthanide–organic frameworks with 4 compounds, based on the "light" or "early" lanthanides Pr, Nd, Sm, and Eu. These compounds show structural motifs that are new and have not been reported yet. We describe their synthesis, crystal structure determination of the Eu-MOF, Rietveld refinement, and in-depth luminescence investigation. In addition, we report the synthesis, crystal structure determination, and luminescence properties of a Nd-MOF based on the 2,5-pyridinedicarboxylate linker. Both linkers used in this study, and the resulting lanthanide–organic frameworks **1**–**5**, are shown in Chart 1.

## EXPERIMENTAL SECTION

**Chemicals.** Lanthanide nitrates $Ln(NO_3)_3{\cdot}xH_2O$, where Ln = Pr, Nd, Sm ($x$ = 6) or Eu ($x$ = 5), were purchased from Aldrich and used without further purification. Triethylenetetramine (TETA), 1,4-benzenedicarboxylic acid (terephthalic acid; 1,4-$H_2$BDC), and 2,5-pyridinedicarboxylic acid (2,5-$H_2$PDC) were purchased from Acros Organics. Solvent grade *N*,*N*-dimethylformamide (DMF), ethanol (EtOH), nitric acid ($HNO_3$), and tetrahydrofuran (THF) were purchased from Carl Roth GmbH.

**Syntheses.** *Synthesis of Compounds* ***1***, ***2***, ***3***, *and* ***4*** *(Terephthalic Acid Linker).* $Pr(NO_3)_3{\cdot}6H_2O$ (130.5 mg, 0.30 mmol) and 1,4-$H_2$BDC (48 mg, 0.30 mmol) were dissolved in a solvent mixture of DMF (30

**Received:** July 16, 2012
**Published:** October 18, 2012

   dx.doi.org/10.1021/ic301544q | *Inorg. Chem.* 2012, 51, 11623−11634

**Chart 1. Chemical Structure of 1,4-Benzenedicarboxylic Acid (Left: Terephthalic Acid, 1,4-$H_2$BDC) and 2,5-Pyridinedicarboxylic Acid (Right: 2,5-$H_2$PDC), the Two Linkers Used in the Lanthanide-MOFs 1−5 Discussed in This Article**

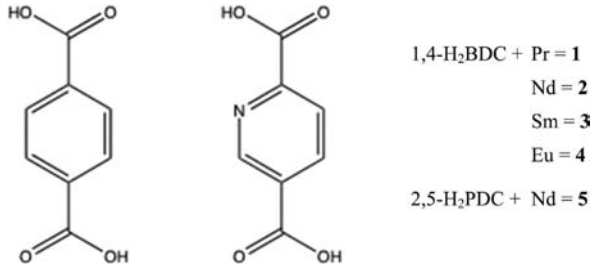


mL), $H_2O$ (6 mL), and EtOH (6 mL) at room temperature. Six drops (about 0.15 mL) of TETA were added to this mixture. $HNO_3$ (6 M) was then added (about 0.5 mL) until the mixture became clear (the solution pH was then about 8). The resulting mixture was left undisturbed at 60 °C for 7 days, after which it was filtered and washed with DMF (10 mL) and THF (10 mL) to yield a green crystalline powder. The yield was 37.4% based on Pr. Anal. Calcd for $C_{33}H_{33}N_3O_{16}Pr_2{\cdot}H_2O$ (**1**): C, 38.58; H, 3.43; N, 4.09%. Found: C, 38.64; H, 3.36; N, 4.63%.

The syntheses for **2**, **3**, and **4** follow the same procedure except that the corresponding lanthanide nitrate salt was used: for **2**, $Nd(NO_3)_3{\cdot}6H_2O$ (131.5 mg, 0.30 mmol); for **3**, $Sm(NO_3)_3{\cdot}6H_2O$ (133 mg, 0.30 mmol); for **4**, $Eu(NO_3)_3{\cdot}5H_2O$ (128 mg, 0.30 mmol). For $C_{33}H_{33}N_3O_{16}Nd_2{\cdot}H_2O$ (**2**) the yield of violet crystalline powder was 39.1% based on Nd. Anal. Calcd: C, 38.33; H, 3.41; N, 4.06%. Found: C, 38.42; H, 3.42; N, 4.65%. For $C_{33}H_{33}N_3O_{16}Sm_2{\cdot}2.5H_2O$ (**3**) the yield was 27.6% based on Sm. Anal. Calcd: C, 36.92; H, 3.57; N, 3.91%. Found: C, 36.33; H, 2.99; N, 4.10%. For $C_{33}H_{33}N_3O_{16}Eu_2{\cdot}H_2O$ (**4**) the yield of white crystalline powder, from which crystals suitable for single crystal X-ray diffraction were harvested, was 42.6% based on Eu. Anal. Calcd: C, 37.76; H, 3.36; N, 4.00%. Found: C, 37.33; H, 2.96; N, 3.52%.

*Synthesis of Compound* ***5*** *(Pyridinedicarboxylic Acid Linker).* $Nd(NO_3)_3{\cdot}6H_2O$ (131 mg, 0.30 mmol) and 2,5-$H_2$PDC (75 mg, 0.45 mmol) were mixed within 5 mL of $H_2O$. After stirring for 30 min, the mixture was placed in a 100 mL Teflon lined reactor and heated at 160 °C in an oven for 3 days. Afterward the resulting solution was slowly cooled to room temperature at 0.1 °C $min^{-1}$. Filtration and washing with $H_2O$ provided the brown crystals suitable for single-crystal X-ray diffraction analysis. The yield was 43.3% based on Nd. Anal. Calcd for $C_{14}H_7N_2O_8Nd{\cdot}H_2O$ (**5**): C, 34.08; H, 1.84; N, 5.68%. Found: C, 34.50; H, 1.45; N, 5.85%.

**Single Crystal X-ray Crystallography.** For the reported structures of compounds **4** and **5**, X-ray intensity data were collected at 100 K on a SuperNova dual source diffractometer equipped with an Atlas CCD detector using Mo K$\alpha$ radiation ($\lambda$ = 0.710 73 Å), and $\omega$ scans. The images were interpreted and integrated with the program CrysAlis PRO from Agilent Technologies.[18] The structures were solved by direct methods and refined by full-matrix least-squares on $F^2$ using the SHELXTL program package.[19,20] Non-hydrogen atoms were anisotropically refined and the hydrogen atoms in the riding mode with temperature factors fixed at 1.2 × $U$(eq) of the parent atoms (1.5 times for methyl and hydroxyl groups). CCDC-891471 and CCDC-891472 contain the supplementary crystallographic data for this paper and can be obtained free of charge via www.ccdc.cam.ac.uk/conts/retrieving.html (or from the Cambridge Crystallographic Data Centre, 12 Union Road, Cambridge CB2 1EZ, U.K.; fax +44-1223-336033; e-mail deposit@ccdc.cam.ac.uk).

**Powder X-ray Diffraction and Refinement.** Powder diffractograms were taken on a powder diffractometer type ARL X'TRA (Thermo Scientific) equipped with a Cu K$\alpha$ ($\lambda$ = 1.5405 Å) tube, goniometer, and Peltier cooled Si(Li) solid state detector in the 2$\theta$ region 5−50° with 0.02° step size and acquisition time per data point of 2.4 s. For Rietveld refinement, the 2$\theta$ region 8−11° from the above diffractograms was recorded once again, in more detail, with 0.005° step size and acquisition time per data point equal to 6s.

The Eu-containing phase, with unit cell containing solely lanthanide ions, was fitted to the experimental data using the MAUD freeware package downloaded from http://www.ing.unitn.it/~maud/index.html, refining first scale factors and background, second the cell parameters, and finally the atomic coordinates.

**Elemental Analysis.** Elemental analyses were carried out on a Thermo Scientific Interscience Flash 2000 organic elemental analyzer. Typically, 2.5 mg of powdered sample was placed into an Ag cup together with $V_2O_5$ catalyst.

**FTIR.** FTIR measurements were taken on a Bruker Equinox 55 FT-IR spectrometer equipped with a DRIFTS-cell. Every measurement was preceded by a background spectrum measurement using KBr powder as reference. All samples were recorded in the 4000−650 $cm^{-1}$ range with a 2 $cm^{-1}$ step size.

**TGA.** Thermogravimetric analyses were performed on a Netzsh STA 449 F3 Jupiter Thermobalance. Typically, 2.5 mg of powder was heated from room temperature to 600 °C at 2 °C $min^{-1}$, under nitrogen athmosphere.

**BET.** Porosity and internal surface were determined with a Micromeritics Tristar 300 surface area and porosity analyzer. Typically, 5 mg of powder was used.

**Photoluminescence Spectroscopy.** Steady state emission and excitation measurements were performed on an Edinburgh Instruments FLSP920 UV−vis−NIR spectrofluorimeter, using a 450 W xenon lamp as the steady state excitation source, a Hamamatsu R928P PMT detector for the visible range, and a Hamamatsu R5509-72 NIR PMT detector for the near-infrared (NIR) range. The excitation and emission spectra have been corrected for detector response and lamp spectrum. Solid powdered samples were put between quartz plates (Starna cuvettes for powdered samples, type 20/C/Q/0.2). Time-resolved measurements were done with a Continuum Surelite I-10 Nd:YAG laser (450 mJ @ 1064 nm), using the third harmonic (355 nm), operating at a pulse frequency of 10 Hz, or with a 60 W xenon microsecond flash lamp, operating at a pulse frequency of 100 Hz.

## RESULTS AND DISCUSSION

**Syntheses of the MOFs.** The synthesis of the terephthalate-based compounds **1**, **2**, **3**, and **4** follows a mild procedure, inspired by the papers by Guo et al. and Na et al.[21,22] No solvothermal conditions are required. Lanthanide nitrate salts and terephthalic acid are dissolved in a mixture of DMF, EtOH, and $H_2O$. After deprotonation with drops of the amine base TETA (about 0.15 mL) and adjustment of the pH to 8 with diluted $HNO_3$, the mixture is left to stand for prolonged time (7 days) at 60 °C, upon which the coordination polymer precipitates. It is recovered after filtering, washing, and drying under vacuum at 50 °C.

Probably the most important difference between our work and the procedures followed by Guo et al. and Na et al. is the fact that we have used four lanthanides that are located in the first half of the lanthanide series: Pr, Nd, Sm, and Eu. These so-called "light" or "early" lanthanides have a larger ionic radius than the "heavy" or "late" lanthanides, which are positioned in the second half of the lanthanide series. Often similarities are encountered *within* either the first or second half of the series, but marked differences can occur between the two halves of the series. Both Guo et al. and Na et al. have reported MOFs based on heavy lanthanides: Tb, Dy, Ho, and Er for Guo et al. and Yb for Na et al.

Apart from different lanthanides used, there are also subtle differences in the synthetic procedures. For example, the reaction temperature in our work is slightly higher (60 °C

instead of 55 °C in the Guo paper). We have also used different amounts of reagent: the Guo paper describes the use of 0.1 mmol of $H_2$BDC linker, 0.1 mmol of lanthanide salt, and a 10:2:2 mL mixture of DMF:EtOH:$H_2O$. We have tripled these amounts. Furthermore, when working with "droplets" of a base solution such as TETA, it is hard to compare the size of the droplets and the speed with which they are added to the reaction medium. The same holds for the addition of $HNO_3$ to adjust the pH again after the addition of the base. The work of Na et al. yields an Yb structure, homologous to the structures reported by Guo et al. However, the solvent mixture described in the Na paper does not contain $H_2O$. Again different quantities of reagent have been used: only 0.06 mmol of $H_2$BDC linker is present and 0.1 mmol of $Yb(NO_3)_3$. The temperature, however, is equal to the one we also applied: 60 °C. Finally, a different base ($MeNH_2$) is used. It seems that the identity of the metal ion, the reaction temperature, and reagent quantities are all parameters of significant importance in coordination polymer synthesis. The fact, however, that a comparable crystal structure was obtained in the papers by Guo et al. and Na et al., even though they used slightly different synthetic methods, suggests that the identity of the metal ion (light vs heavy lanthanide, meaning large vs small ionic radius) is of more importance than the exact reaction conditions, as the crystal structure reported in this work (see further) is significantly different from those reported in the Guo and Na papers.

Pyridinedicarboxylate-based compound **5** is prepared through a typical hydrothermal method in an autoclave at 160 °C.[23,24] Here, we used the same procedure as reported by Huang et al. and Qin et al.: after mixing the dicarboxylic acid with the lanthanide salt in water, the mixture becomes clear upon heating. No additional deprotonating reagents are required. After three days, crystals precipitate and are readily harvested after slowly cooling the mixture. The crystal structure obtained here (see further) is homologous to the ones reported in the Huang and Qin papers.

**Description of Crystal Structures.** The structures of compound **4** and **5** were determined by single crystal X-ray diffraction. Table 1 summarizes the most important crystallographic data.

Compound **4** crystallized in the centrosymmetric triclinic space group $P\bar{1}$. To the best of our knowledge, this reported structure is *not* isostructural to any other previously deposited structure in the CSD (Cambridge Structural Database).[25] The asymmetric unit is composed of two crystallographically distinct Eu(III) metal centers, three coordinating 1,4-$BDC^{2-}$ (1,4-benzenedicarboxylate) ligands, two coordinating DMF molecules, one coordinating water molecule, and one DMF solvent molecule.

A first Eu(III) ion is octacoordinated with six oxygen atoms from the carboxylate groups of six different monodentately coordinating 1,4-$BDC^{2-}$ ligands (Eu−O distances ranging from 2.322(8) to 2.402(7) Å), one DMF oxygen atom (Eu−O distance of 2.497(11) Å), and one water molecule (Eu−O distance of 2.514(8) Å) (Figure 1). The second Eu(III) ion is octacoordinated as well, but with seven oxygen atoms, from the carboxylate groups of five monodentately and one bidentatetely coordinating 1,4-$BDC^{2-}$ ligands, (Eu−O distances ranging from 2.307(7) to 2.598(8) Å) and from one DMF oxygen atom (Eu−O distance of 2.397(10) Å) (Figure 2). For both Eu(III) ions, the coordination environment can be considered a distorted square antiprism.

**Table 1. Crystallographic Data for Compounds 4 and 5**

| | 4 | 5 |
|---|---|---|
| molecular formula | $C_{33}H_{33}Eu_2N_3O_{16}$ | $C_{14}H_7N_2NdO_8$ |
| fw (g $mol^{-1}$) | 1031.56 | 475.46 |
| cryst dimensions ($mm^3$) | 0.21 × 0.14 × 0.11 | 0.40 × 0.20 × 0.20 |
| cryst syst | triclinic | orthorhombic |
| space group | $P\bar{1}$ (No. 2) | *Pbcn* (No. 60) |
| *a* (Å) | 11.0552(7) | 9.9599(8) |
| *b* (Å) | 11.0713(6) | 8.7592(8) |
| *c* (Å) | 17.6488(10) | 15.7875(16) |
| $\alpha$ (deg) | 93.084(5) | 90.00 |
| $\beta$ (deg) | 104.429(5) | 90.00 |
| $\gamma$ (deg) | 119.032(6) | 90.00 |
| *V* ($Å^3$) | 1789.8(2) | 1377.3(2) |
| *Z* | 2 | 4 |
| $\rho_{calcd}$ (g $cm^{-3}$) | 1.914 | 2.293 |
| $2\theta_{max}$ (deg) | 50.70 | 52.72 |
| *T* (K) | 100(2) | 100(2) |
| *F*(000) | 1012 | 916 |
| measured reflns | 11 627 | 9380 |
| unique reflns | 9981 | 1410 |
| obsd reflns ($I > 2\sigma(I)$) | 7985 | 1252 |
| params refined | 494 | 115 |
| R1 | 0.0672 | 0.0208 |
| wR2 | 0.1891 | 0.0547 |
| R1 (all data) | 0.0842 | 0.0240 |
| wR2 (all data) | 0.2094 | 0.0577 |
| GOF | 1.092 | 1.144 |
| $\mu$ ($mm^{-1}$) | 3.551 | 3.823 |
| CCDC entry | CCDC-891471 | CCDC-891472 |

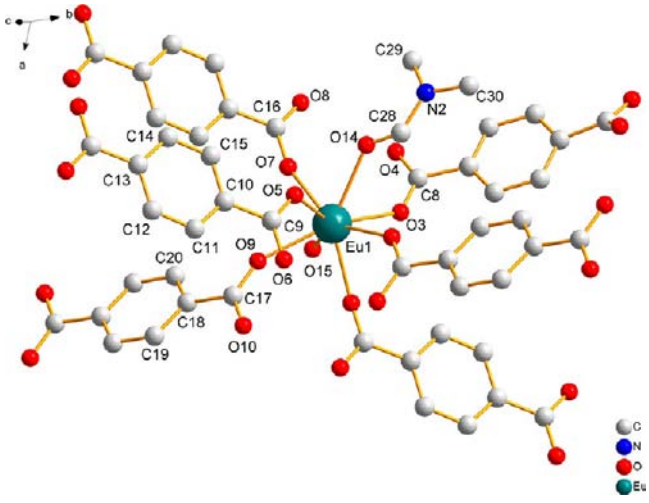


**Figure 1.** Coordination environment of the first Eu(III) ion "Eu1" in the crystal structure of compound **4**, with atom labeling scheme of the asymmetric unit. Hydrogen atoms are omitted for clarity.

In the packing, Eu1 is connected through four bidentately 1,4-$BDC^{2-}$ ligands to its symmetry equivalent Eu1[1 − *x*,1 − *y*,1 − *z*] (inversion center), whereas Eu2 is connected through two bridging and two bidentately 1,4-$BDC^{2-}$ ligands to its symmetry equivalent Eu2[−*x*, −*y*, −*z*], the latter leading to an edge-sharing dimer. On their turn, these metallic dimers are linked to each other through two bidentately 1,4-$BDC^{2-}$ ligands, leading to 4-centered secondary building units (SBU) (Figure 3). These SBUs are further assembled into 1D chains, along the [1, 1, 1] direction. These chains are cross-linked by 1,4-$BDC^{2-}$


dx.doi.org/10.1021/ic301544q | *Inorg. Chem.* 2012, 51, 11623−11634

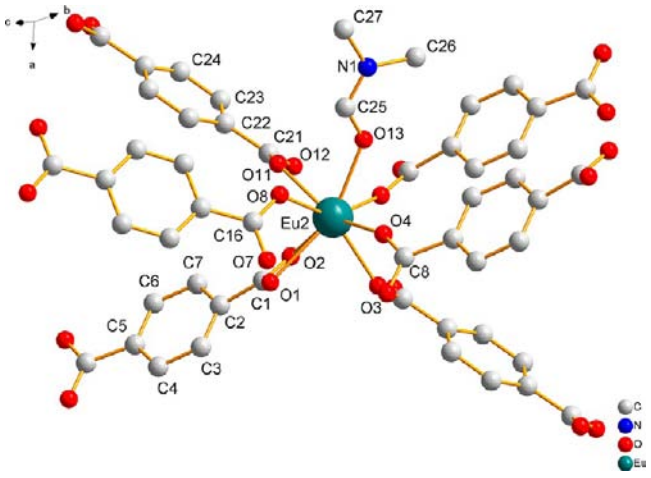


**Figure 2.** Coordination environment of the second Eu(III) ion "Eu2" in the crystal structure of compound **4**, with atom labeling scheme of the asymmetric unit. Hydrogen atoms are omitted for clarity.

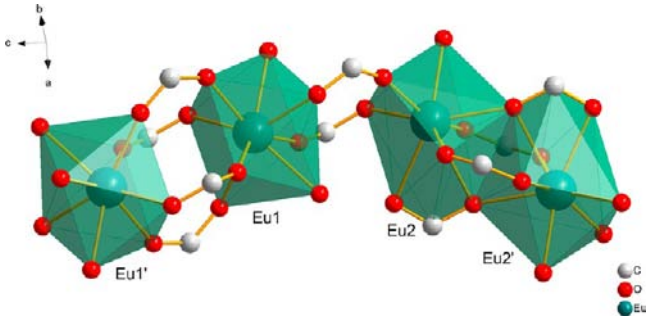


**Figure 3.** Four-centered secundary building unit (SBU) in the structure of compound **4**, showing coordination polyhedra and atom-labeling of the four Eu ions.

ligands in the (1, −1, 0) plane and (−1, 0, 1) plane, building up a 3D network, with 11.23 Å by 11.07 Å (side lengths, measured between the Eu atoms) rhombic channels along the [1, 1, 1] direction (Figure 4), with a void volume of 35.1% of the unit cell volume or 628.68 Å$^3$ (DMF molecules not taken into account), and with a void volume of 36.7% of the unit cell volume of 657.72 Å$^3$ (DMF and coordinated water molecule not taken into account), calculated with the program Mercury CSD 2.4.[26] The coordinating, as well as the solvent DMF, molecules are pointing into these channels (Figure 5).

The only other structure found in the CSD, containing a Eu(III) ion, 1,4-BDC$^{2-}$, and DMF, contains also binuclear Eu(III) centers as building blocks. However, each Eu(III)-center is nonacoordinated, from three bidentately and one monodentately coordinating 1,4-BDC$^{2-}$ ligands, one DMF, and one water molecule. The coordination is considered a distorted tricapped trigonal prism, and a 3D interpenetrating coordination polymer is formed.[27] Gd, Dy, Er, and Tm complexes, isostructural to the latter Eu-complex, also exist, with the Er complex slightly differing in the coordination of the binuclear Er clusters, which are bridged by two mono(bidentate) 1,4-BDC$^{2-}$ carboxylates and further coordinated by two bidentate 1,4-BDC$^{2-}$ carboxylates, one DMF, and one water molecule in a distorted square antiprism geometry.[28−30]

Other, different Ln-containing coordination polymers with 1,4-BDC$^{2-}$ and DMF ligands were previously reported: containing one Er(III) center, coordinated by seven O-atoms (from six monodentate 1,4-BDC$^{2-}$ and one DMF), showing one coordination mode of 1,4-BDC$^{2-}$, and with 1,4-BDC$^{2-}$ linking four Er(III) atoms using its two bridging carboxylate groups.[31] Another five isostructural Ln-complexes were reported, with Ln = Tb, Dy, Ho, and Er (Guo et al.)[21] and Ln = Yb (Na et al.),[22] showing three different coordination Ln-centers, and forming a 3D network built up from discrete, as well as infinite SBUs, leading to pseudochains rather than infinite chains.

Another three other isostructural Ln-complexes, with Ln = La, Ce, and Nd, were reported, showing six crystallographically different Ln-ions, with three different types of coordination numbers, leading to 3D Ln-BDC MOFs.[32]

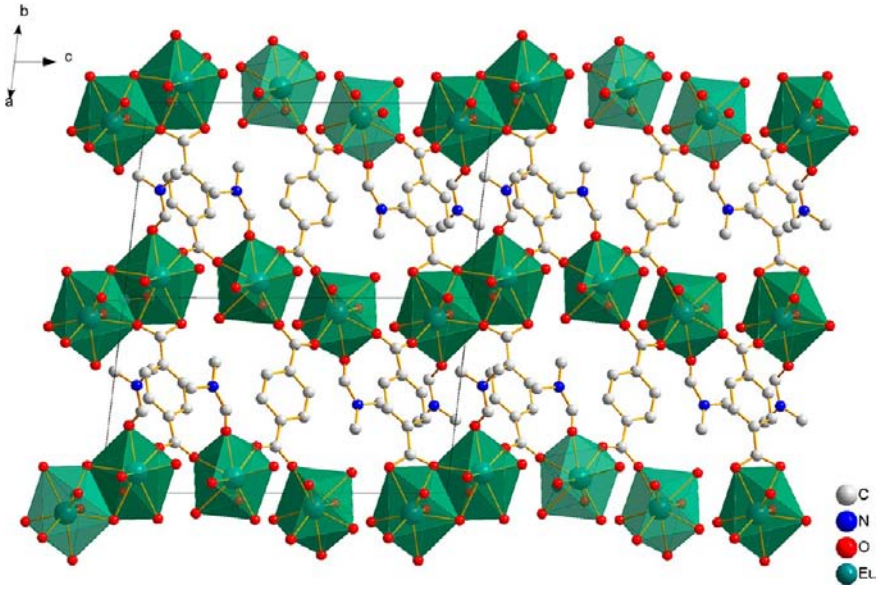


**Figure 4.** Packing diagram, showing the 3D framework of the structure of compound **4** down the [1, 1, 0] direction, with coordination polyhedra indicated. Only 1,4-BDC$^{2-}$ ligands, connecting the Eu(III) centers in the [0, 1, 0] direction, as well as the coordinating DMF ligands are shown. Hydrogen atoms are omitted for clarity.


dx.doi.org/10.1021/ic301544q | *Inorg. Chem.* 2012, 51, 11623−11634

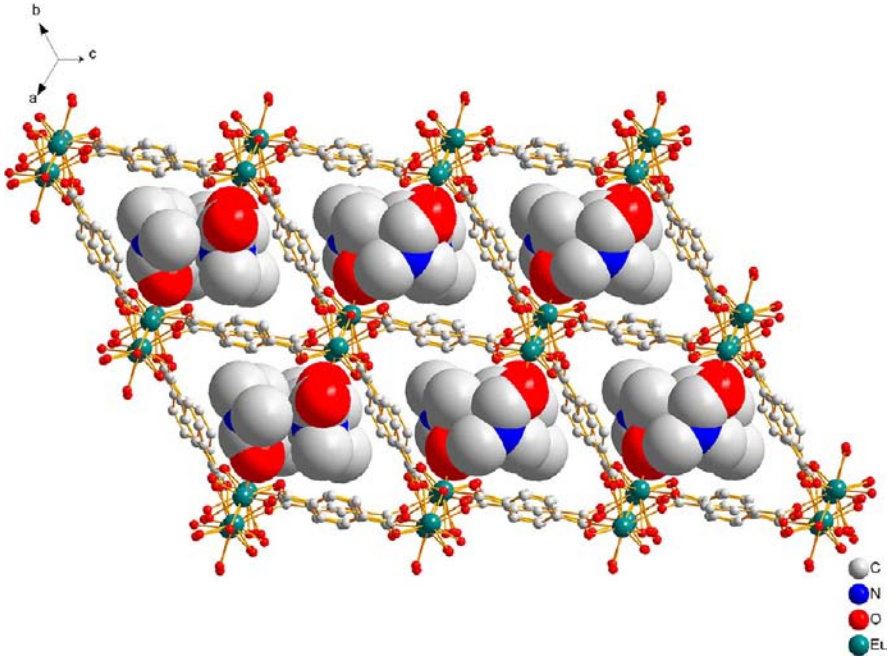


**Figure 5.** Packing diagram, showing the 3D framework of the structure of compound **4**, down the [1, 1, 1] direction, showing the 1D rhombic channels, in which the coordinated DMF and water molecules, as well as the guest DMF molecules, are represented in space fill mode.

Compound **5** crystallized in the orthorhombic space group *Pbcn*. The asymmetric unit consists of one Nd(III) metal center, positioned on the 2-fold axis (occupancy = 0.5) and one 2,5-$PDC^{2-}$ (2,5-pyridinedicarboxylate) ligand. The structure is homologous to the previously reported Eu(III), Tb(III), Gd(III), and Sm(III) structures.[23,24,33]

The Nd(III) ion is octacoordinated with six oxygen atoms and two nitrogen atoms. The Nd(III) coordination environment can be considered as a distorted square antiprism. Two 2,5-$PDC^{2-}$ ligands coordinate bidentately to the Nd(III), through their pyridine nitrogen atom and one carboxylate oxygen atom, while four other 2,5-$PDC^{2-}$ ligands are monodentately coordinating through their pyridine nitrogen atom and a carboxylate oxygen atom (Figure 6). The Nd−N bond distance is 2.618(2) Å, while there are three different symmetry-related Nd−O bond distances: 2.413(2), 2.376(2), and 2.445(2) Å, respectively. Each 2,5-$PDC^{2-}$ ligand coordinates to three Nd(III) ions, i.e., the two oxygen atoms of the first carboxylate coordinate each to a Nd(III) ion (monobidentate), while one oxygen atom of the second carboxylate coordinates to a third Nd(III) ion (monodendate).

To satisfy the charge equilibrium of the total coordination polymer, half of the 2,5-$PDC^{2-}$ ligands are protonated: a hydrogen atom (occupancy = 0.5) was modeled on the O4 carboxylate atom of the 2,5-$PDC^{2-}$. Hence, an intermolecular hydrogen bond is formed between the carboxylate atom O4 of a 2,5-$PDC^{2-}$ ligand and O4 of a symmetry equivalent ligand (O···O distance of 2.404(3) Å). As a matter of fact, this hydrogen atom could be located from a difference Fourier electron density map, where an additional peak was observed on the 2-fold symmetry axis between carboxylate atom O4 and the symmetry equivalent O4 $[-x, y, -{}^{1}/_{2} - z]$.

The 3D framework can be considered as built up by layers of octacoordinated Nd(III) metal centers in the (0, 0, 1) plane, linked by layers of the 2,5-$PDC^{2-}$ ligands in the [0, 0, 1] direction (Figure 7).

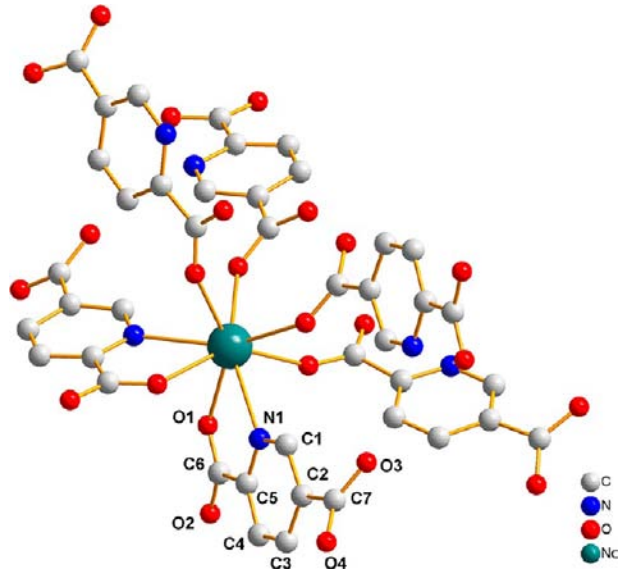


**Figure 6.** Coordination environment of the Nd(III) ion in the crystal structure of compound **5**, with labeling scheme of the asymmetric unit. Hydrogen atoms are omitted for clarity.

**Powder X-ray Diffraction and Rietveld Refinement.** Bragg−Brentano ($\theta$, $2\theta$) XRD spectra were measured on the synthesized powders. On the basis of the resolved crystal structure for Eu-MOF **4**, the ($\theta$, $2\theta$) XRD spectrum was calculated (see Figure 8a). The peaks at low Bragg angle are the result of the diffraction of lattice planes containing the lanthanide atoms as shown in Figure 9, where these lattice planes are indicated. When removing the low $Z$ atoms (C, N, O, and H) from the structure, one notices that the overall XRD spectrum is hardly modified in the low angle range (see Figure 8b), which is understandable from the structure and the fact that the atomic scattering factor for the lanthanide atoms is much higher as compared to the low $Z$ atoms. On the basis of


dx.doi.org/10.1021/ic301544q | *Inorg. Chem.* 2012, 51, 11623−11634

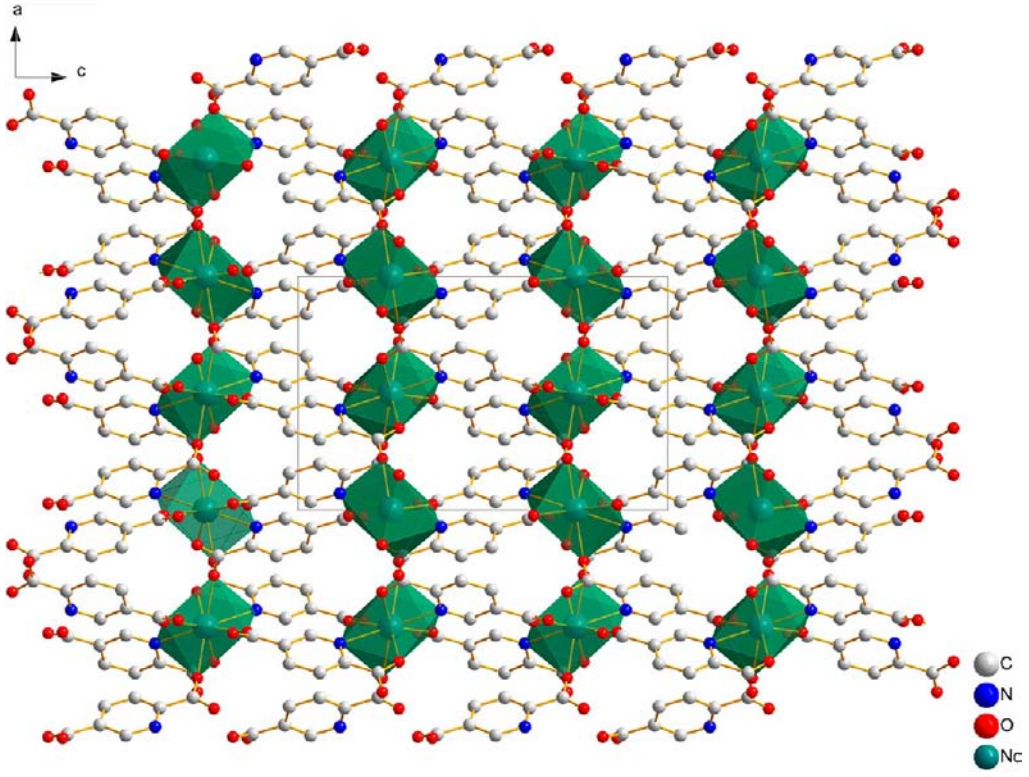


**Figure 7.** Packing diagram, showing the 3D framework of the structure of compound **5**, down the crystallographic *b*-axis, with coordination polyhedra indicated. Hydrogen atoms are omitted for clarity.

this result, the following assumption was made to retrieve the lattice parameters for the different 1,4-$BDC^{2-}$ based MOFs by Rietveld refinement: First, it was assumed that the structure of the 1,4-$BDC^{2-}$ based MOFs **1**, **2**, and **3** was similar to the Eu based material **4**. This allows us to retrieve the lattice parameters based on the peak positions. However, to solve the problem of the intensity calculation in the Rietveld refinement, we assumed that the intensity for the low angle Bragg lines was solely defined by the positions of the lanthanide atoms; i.e., the low *Z* elements were excluded from the calculations. This method allows us to calculate correctly the cell parameters, without the need to solve the complete powder structure. The XRD patterns together with the fits are shown for the different elements in Figure 8, parts c to f. On the basis of the agreement between the fits and the experimental curves, it is clear that the unit cells are identical for each of the lanthanide-MOFs **1** to **4**, pointing to a highly isostructural relationship between these MOFs.

Figure 10 shows the trends in the lattice parameters as a function of the increasing cation radius of the lanthanide ion. The cation radius was taken from R. D. Shannon.[34] The correlation between the lattice parameters and the cation radius was statistically tested. Only for the *a*-parameter was a significant linear decrease as a function of the increasing cation radius found (Kendall rank correlation test, significance level 97.5%). Also a significant decrease, although not linear, of the angle between the *a* and *b* axis, i.e., $\gamma$, is noticed as a function of increasing cation radius (Kendall rank correlation test, significance level 95%).

**IR, TGA, BET.** In the IR spectrum of **4** the characteristic symmetric and asymmetric stretching vibrations from the deprotonated carboxylic acids are found at 1313 and 1580 $cm^{-1}$, respectively. A peak at 828 $cm^{-1}$ corresponds to the 1,4-benzene substitution pattern. The bands of the aromatic benzene skeleton vibration are found at 1512 $cm^{-1}$. The large peak at 1624 $cm^{-1}$ corresponds to the coordinating DMF amide carbonyl. At 3061 $cm^{-1}$ the aromatic C−H stretch is present. The IR spectra for compounds **1**, **2**, and **3** are analogous to that of compound **4** (see Figure S1 in the Supporting Information). In the IR spectrum for **5**, the broad O−H stretch for H-bonded carboxylic acid hydrogen appears in the 3500−2500 $cm^{-1}$ region. The protonated and both the symmetric and asymmetric deprotonated carboxylic acid group stretch vibrations are visible at 1963 $cm^{-1}$, and at 1594 and 1293 $cm^{-1}$, respectively (see Figure S2 in the Supporting Information).

The thermal stability of the compounds has been investigated by thermogravimetric analysis (see Figure S3 in the Supporting Information). The TGA analysis results for compound **4** are representative for the other compounds **1**, **2**, and **3** and are discussed here. The first weight loss for **4**, amounting to 6.2%, occurs between 80 and 120 °C and implies the loss of coordinated and guest $H_2O$ molecules (calcd 3.43%). A second weight loss of 8.9% is observed between 190 and 240 °C, corresponding to the removal of a guest DMF molecule (calcd 6.9%). Beyond 390 °C the coordination polymer decomposes, leaving 34.6% of the initial weight remaining as $Eu_2O_3$ (calcd 33.4%).

The terephthalate-based MOFs were also submitted for BET analysis. The found BET surfaces are 3.4138 $m^2/g$ for **1**, 5.1376 $m^2/g$ for **2**, 2.6876 $m^2/g$ for **3**, and 2.9818 $m^2/g$ for **4**. These surfaces are low, describing in essence the surface of the outer area of the MOF structure. One therefore has to conclude that these MOFs **1**−**4** can be considered as not porous. This can indeed be seen in the crystal structure of **4**, where the coordinating DMF molecules, together with solvent (guest)


dx.doi.org/10.1021/ic301544q | *Inorg. Chem.* 2012, 51, 11623−11634

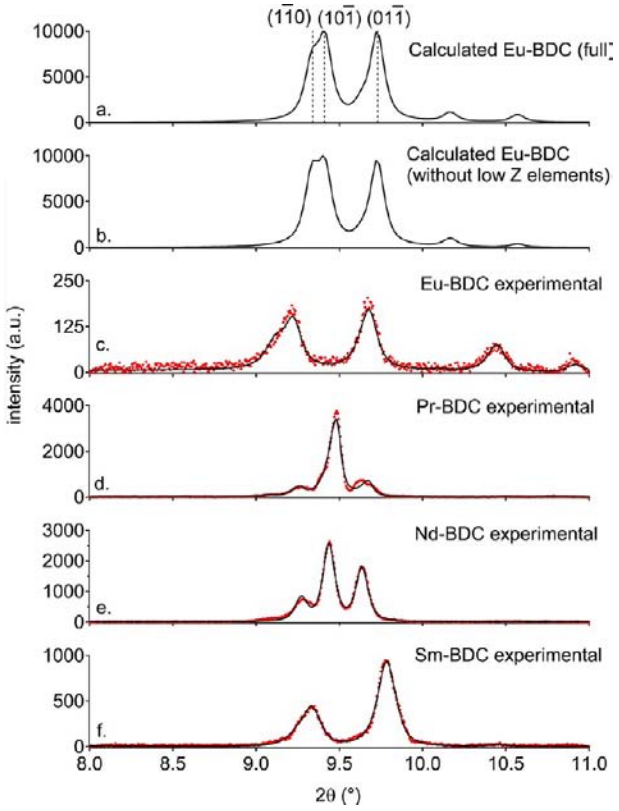


**Figure 8.** Overview of the calculated (solid black line) and experimental (red dots) Bragg–Brentano ($\theta$, $2\theta$) XRD patterns. (a) Calculated pattern for **4** based on the crystal structure (calculation performed using Mercury 3.0). (b) Calculated pattern for **4** based on the crystal structure, excluding the low $Z$ elements in the calculation (calculation performed using Mercury 3.0). (c) Experimental and simulated pattern (using MAUD) for **4**. The shift as compared to the calculated pattern is due to the difference in temperature (100 K in part a, RT in part c). (d) Experimental and simulated pattern (using MAUD) for **1**. (e) Experimental and simulated pattern (using MAUD) for **2**. (f) Experimental and simulated pattern (using MAUD) for **3**.

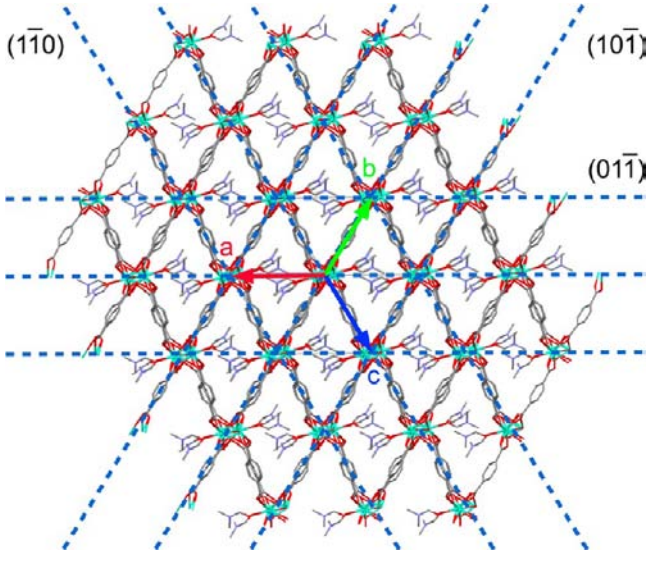


**Figure 9.** Crystal structure of **4** along the [1, 1, 1] direction, together with the lattice planes containing Eu atoms which have a strong contribution to the Bragg–Brentano ($\theta$, $2\theta$) XRD spectra at low angles.

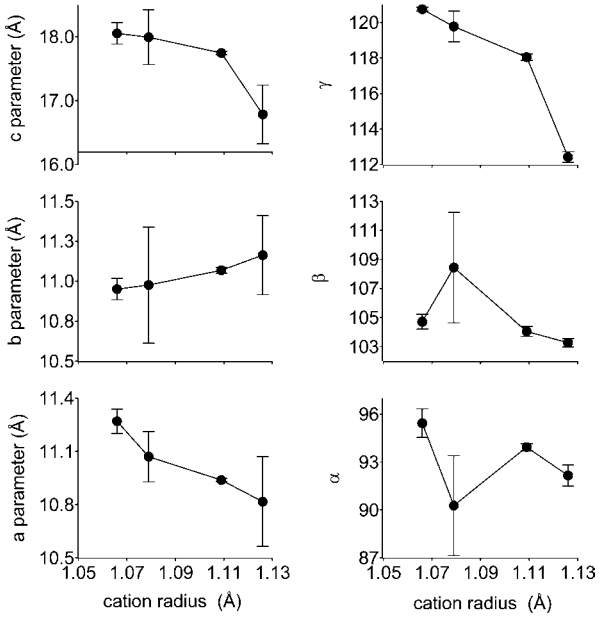


**Figure 10.** Lattice parameters as a function of the cation radius of the lanthanide ion.

DMF molecules and a coordinating water molecule, in fact fill up the voids that would otherwise have been responsible for the porosity of the resulting material. The DMF guest molecules are notoriously hard to remove, but the DMF molecules that coordinate to the Eu-ions are even harder to remove. This means that, in practice, these MOFs cannot be considered to be porous materials, even though the void volume can be calculated, hypothetically removing the molecules that are present in the channels.

**Luminescence Measurements.** Compounds **1**–**5** all contain lanthanides, so they could have interesting luminescent properties, as the trivalent lanthanide ions are well-known for their linelike and color-pure emission, both in the UV–vis and the near-infared regions of the electromagnetic spectrum.[35–37] Indeed, luminescent lanthanide–organic frameworks are frequently reported in scientific literature, often in high-impact journals.[17,38–40]

Even though the majority of the reported lanthanide-MOFs are based on di- or tricarboxylate linkers, which are not necessarily the best ligands for sensitizing the lanthanide ions' luminescence, there have already been very promising results nevertheless. The materials reported in this Article all show the typical lanthanide-based luminescence too, although weak for the neodymium-compounds **2** and **5**, but reasonably strong for the praseodymium and samarium compounds **1** and **3** and strong enough to be seen by the naked eye under illumination with a standard laboratory UV-lamp for the europium compound **4** (see Table of Contents graphic).

The combined excitation–emission spectra for compounds **1**–**5** are given in Figures 11–14, and the assignment of the observed electronic transitions can be found in Table 2. The presence of the typical 4f–4f transitions is obvious from looking at the emission spectra.[41,42] For europium compound **4**, this is not very remarkable, as this is by far the most widely studied luminescent lanthanide ion, showing luminescence that can be so intense that it can be seen under sunlight illumination. It is nevertheless interesting to point out that transitions in the excitation spectrum of **4** are identified as


dx.doi.org/10.1021/ic301544q | Inorg. Chem. 2012, 51, 11623–11634

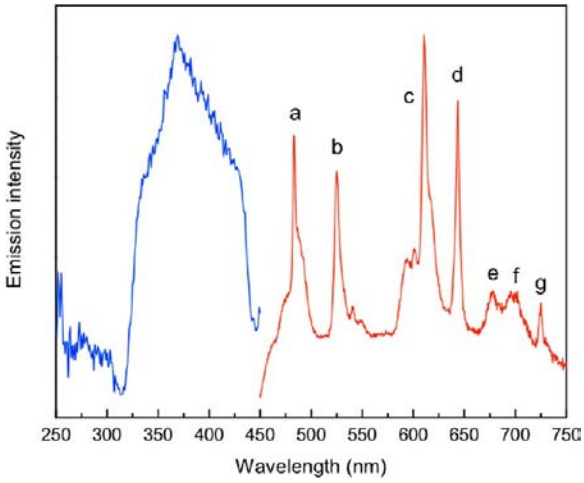


**Figure 11.** Excitation spectrum (blue, monitored at 643.5 nm) and emission spectrum (red, excited at 300 nm) of Pr-MOF **1**. For assignment of the electronic transitions labeled a–g, see Table 2.

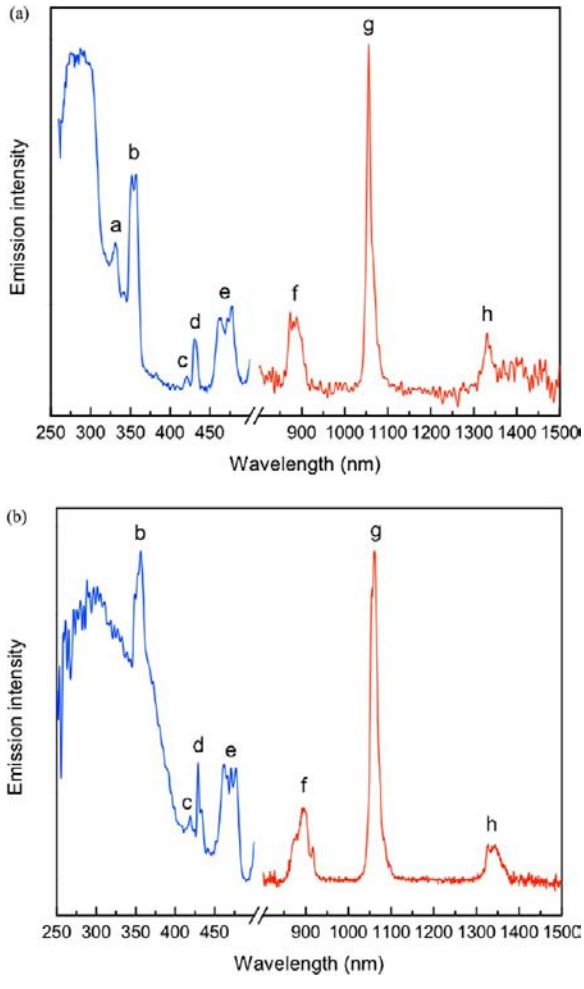


**Figure 12.** Excitation spectrum (blue, monitored at 1056 nm for **2** and at 1061 nm for **5**) and emission spectrum (red, excited at 300 nm for both **2** and **5**) of Nd-MOFs **2** (a) and **5** (b). For assignment of the electronic transitions labeled a–h, see Table 2.

coming from the $^7F_0$ ground level, as well as from the first excited state $^7F_1$. This can be explained by looking at the energy level scheme in Figure 15: the $^7F_1$ level is only about 360 $cm^{-1}$

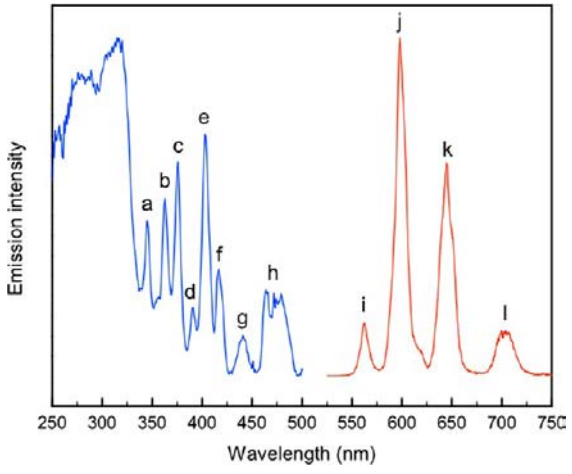


**Figure 13.** Excitation spectrum (blue, monitored at 598.1 nm) and emission spectrum (red, excited at 300 nm) of Sm-MOF **3**. For assignment of the electronic transitions labeled a-l, see Table 2.

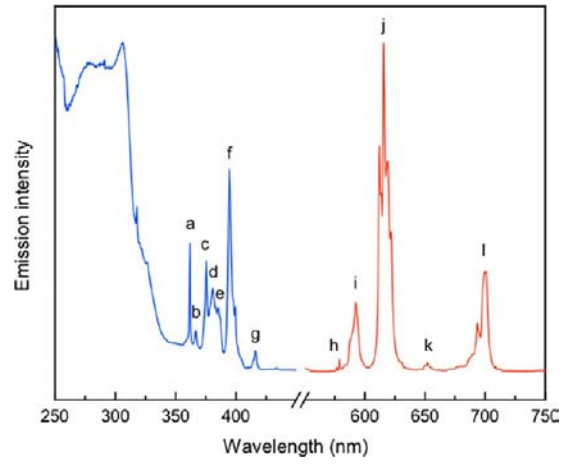


**Figure 14.** Excitation spectrum (blue, monitored at 616.0 nm) and emission spectrum (red, excited at 300 nm) of Eu-MOF **4**. For assignment of the electronic transitions labeled a-l, see Table 2.

above the $^7F_0$ ground state, which means that, in accordance with the Boltzmann distribution of a number of particles at a given temperature, about one-third of the valence electrons in the europium ions are in the $^7F_1$ excited state, leaving two-thirds in the $^7F_0$ ground state.

Far less common than europium luminescence are the spectra of samarium compound **3**, as this ion is much harder to persuade to luminesce than europium or terbium, another widely studied lanthanide ion. The near-infrared (NIR) emission of the trivalent neodymium ion in materials **2** and **5** has also been reported before in Nd-containing MOFs, showing the typical 1064 nm (or thereabout) line which is used in a Nd:YAG laser. To the best of our knowledge, though, this is only the second time that praseodymium luminescence is reported in a carboxylate-based Pr-containing MOF such as **1**. Very recently, a paper was published by Feng et al. describing a praseodymium-containing carboxylate MOF based on deprotonated 2-ethyl-1*H*-imidazole-4,5-dicarboxylic acid and oxalic acid as linkers. In this paper, a concise emission spectrum is shown, albeit less extended than ours, but the paper does not contain an excitation spectrum.[43] Trivalent praseodymium has two emissive electronic states: the $^3P_0$ level, located at about 20


dx.doi.org/10.1021/ic301544q | *Inorg. Chem.* 2012, 51, 11623–11634

Table 2. Assignment of Labeled Electronic Transitions shown in Figures 11 − 14 (Based on Carnall et al.)[49,50]

| excitation | | | | | emission | | | |
|---|---|---|---|---|---|---|---|---|
| | wavelength (nm) | energy ($cm^{-1}$) | transition | | | wavelength (nm) | energy ($cm^{-1}$) | transition |
| | | | Pr-MOF **1** | | | | | |
| | no f−f transitions observed | | | | a | 483.3 | 20 690 | $^3P_0 \rightarrow$ $^3H_4$ |
| | | | | | b | 525.1 | 19 045 | $^3P_0 \rightarrow$ $^3H_5$ |
| | | | | | c | 610.6 | 16 375 | $^3P_0 \rightarrow$ $^3H_6$ |
| | | | | | | | | $^1D_2 \rightarrow$ $^3H_4$ |
| | | | | | d | 643.6 | 15 535 | $^3P_0 \rightarrow$ $^3F_2$ |
| | | | | | e | 677.8 | 14 755 | $^1D_2 \rightarrow$ $^3H_5$ |
| | | | | | f | 697.2 | 14 345 | $^3P_0 \rightarrow$ $^3F_3$ |
| | | | | | g | 724.9 | 13 795 | $^3P_0 \rightarrow$ $^3F_4$ |
| | | | Nd-MOF **2** | | | | | |
| a | 330.8 | 30 230 | $^2L_{15/2}$, $^4D_{7/2}$, $^2I_{13/2}$ | $\leftarrow$ $^4I_{9/2}$ | f | 884.0 | 11 310 | $^4F_{3/2} \rightarrow$ $^4I_{9/2}$ |
| b | 354.4 | 28 220 | $^4D_{3/2}$, $^4D_{5/2}$, $^2I_{11/2}$, $^4D_{1/2}$ | | g | 1055.9 | 9470 | $^4I_{11/2}$ |
| c | 420.8 | 23 760 | $^2D_{5/2}$ | | h | 1330.8 | 7515 | $^4I_{13/2}$ |
| d | 430.9 | 23 210 | $^2P_{1/2}$ | | | | | |
| e | 469.1 | 21 320 | $^4G_{11/2}$, $^2D_{3/2}$, $^2P_{3/2}$, $^2G_{9/2}$, $^2K_{15/2}$ | | | | | |
| | | | Sm-MOF **3** | | | | | |
| a | 344.8 | 29 000 | $^4D_{7/2}$ | $\leftarrow$ $^6H_{5/2}$ | i | 562.6 | 17 775 | $^4G_{5/2} \rightarrow$ $^6H_{5/2}$ |
| b | 362.8 | 27 560 | $^4D_{3/2}$, $^4D_{5/2}$, $^6P_{5/2}$ | | j | 598.1 | 16 720 | $^6H_{7/2}$ |
| c | 376.0 | 26 595 | $^6P_{7/2}$ | | k | 645.0 | 15 505 | $^6H_{9/2}$ |
| d | 390.7 | 25 600 | $^4L_{15/2}$ | | l | 702.9 | 14 225 | $^6H_{11/2}$ |
| e | 403.2 | 24 805 | $^6P_{3/2}$ | | | | | |
| f | 416.8 | 23 995 | $^6P_{5/2}$, $^4P_{5/2}$ | | | | | |
| g | 441.2 | 22 665 | $^4G_{9/2}$, $^4M_{17/2}$ | | | | | |
| h | 472.0 | 21 185 | $^4I_{13/2}$, $^4I_{11/2}$, $^4M_{15/2}$ | | | | | |
| | | | Eu-MOF **4** | | | | | |
| a | 362.1 | 27 620 | $^5D_4$ | $\leftarrow$ $^7F_0$ | h | 579.0 | 17 270 | $^5D_0 \rightarrow$ $^7F_0$ |
| b | 367.0 | 27 250 | $^5D_4$ | $\leftarrow$ $^7F_1$ | i | 592.5 | 16 880 | $^7F_1$ |
| c | 375.4 | 26 640 | $^5G_4$ | $\leftarrow$ $^7F_0$ | j | 616.0 | 16 235 | $^7F_2$ |
| d | 380.6 | 26 275 | $^5G_2$ | $\leftarrow$ $^7F_0$ | k | 652.3 | 15 330 | $^7F_3$ |
| e | 385.4 | 25 950 | $^5G_2$ | $\leftarrow$ $^7F_1$ | l | 700.0 | 14 285 | $^7F_4$ |
| f | 394.4 | 25 355 | $^5L_6$ | $\leftarrow$ $^7F_0$ | | | | |
| g | 416.4 | 24 015 | $^5D_3$ | $\leftarrow$ $^7F_1$ | | | | |
| | | | Nd-MOF **5** | | | | | |
| a | not observed | | | | f | 896.0 | 11 160 | $^4F_{3/2} \rightarrow$ $^4I_{9/2}$ |
| b | 356.3 | 28 070 | $^4D_{3/2}$, $^4D_{5/2}$, $^2I_{11/2}$, $^4D_{1/2}$ | $\leftarrow$ $^4I_{9/2}$ | g | 1061.3 | 9420 | $^4I_{11/2}$ |
| c | 418.6 | 23 890 | $^2D_{5/2}$ | | h | 1335.0 | 7490 | $^4I_{13/2}$ |
| d | 429.0 | 23 310 | $^2P_{1/2}$ | | | | | |
| e | 468.5 | 21 345 | $^4G_{11/2}$, $^2D_{3/2}$, $^2P_{3/2}$, $^2G_{9/2}$, $^2K_{15/2}$ | | | | | |

700 $cm^{-1}$, and the $^1D_2$ level at about 16 400 $cm^{-1}$ (see Figure 15 for a simplified electronic energy level scheme). The fact that emission can occur from both levels can make the interpretation of a Pr(III) emission spectrum rather cumbersome. We have nevertheless made an attempt at assigning the correct transitions to the observed peaks in the emission spectrum (Table 2).

The excitation spectra of compounds **2**−**5** all show 4f−4f transitions as well, aside from a high-energy broad band centered at about 300 nm. The broad band at about 300 nm indicates that part of the excitation light is absorbed by the carboxylate linker and subsequently transferred to the lanthanide ion, which then loses the energy by emitting light at its typical wavelengths. As such, the carboxylate linker serves as an antenna, harvesting part of the excitation light for enhanced lanthanide emission; hence, this is called "the antenna effect". The fact that also 4f−4f transitions are seen in the excitation spectra of **2**−**5**, however, and the fact that these are comparable in intensity to the broad band at 300 nm, indicates that the carboxylate linker is not a very good sensitizer for lanthanide luminescence (otherwise the intensity of the broad band would be several orders of magnitude larger than the 4f−4f transitions, which could even be indistinguishable in the excitation spectrum). As a result, the luminescence shown by compounds **2**−**5** can just as well be obtained by exciting the lanthanide ion directly in its $^{2S+1}L_J$ electronic energy levels, provided that these are at high enough energy to allow the typical (longer wavelength) lanthanide emission to occur.

The reason for the poor antenna properties of the carboxylate linker can probably be found in the fact that its triplet level is most likely at too high energy for efficient energy transfer to the emissive states of the lanthanide ions. We have not been able to determine the triplet level of the terephthalate linker ourselves (as our setup did not yet allow measurement of low-temperature emission spectra), but we have been able to find a value for this triplet energy in literature: Hilder and co-


dx.doi.org/10.1021/ic301544q | Inorg. Chem. 2012, 51, 11623−11634

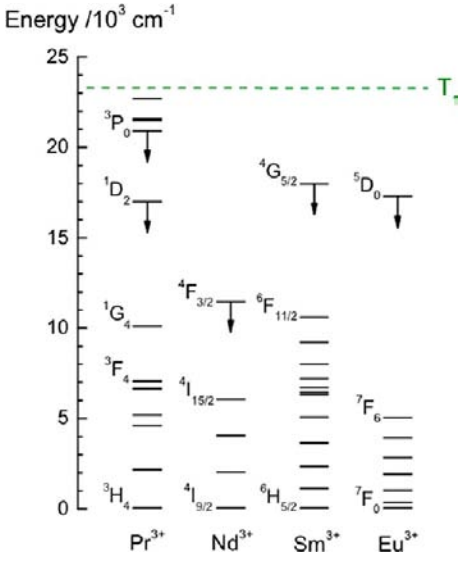


**Figure 15.** Simplified energy level diagram showing the most important $^{2S+1}L_J$ energy levels of $Pr^{3+}$, $Nd^{3+}$, $Sm^{3+}$, and $Eu^{3+}$ (based on the historical work of W. T. Carnall),[49,50] together with the triplet level $T_1$ of the 1,4-$BDC^{2-}$ linker.[44].

workers have determined it to be 23 256 $cm^{-1}$ (we have indicated the terephthalate triplet level with a green dashed line in Figure 15, labeled $T_1$).[44] It can be seen from Figure 15 that the energy gap between this triplet level and the emissive levels of Nd(III), Sm(III), and Eu(III) is large, giving nonradiative relaxation pathways ample opportunity to channel away the energy rather than transferring it to the Ln(III) ion.

The situation for the praseodymium-MOF **1** is different. From Figure 11, two things can be learned: first, the 4f−4f transitions in the emission spectrum seem to be superimposed on a broad, featureless emission band, whereas this was not the case in the emission spectra of the other compounds; second, the excitation spectrum does not contain any 4f−4f transition, but instead of that, contains a broad band located at about 375 nm. These observations can be understood from looking at the energy level diagram in Figure 15. For Pr-MOF **1**, the difference in energy between the terephthalate triplet level and the accepting energy levels of the Pr(III) ion is now rather small, allowing back-energy-transfer from the Pr(III) levels to the triplet level of the linker. As a consequence, this linker now loses part of its energy by showing phosphorescence, which can be seen as the broad band under the 4f−4f lines in the emission spectrum. Thus, one has to conclude that whereas the linker triplet level energy is too high for efficient sensitization of Nd(III), Sm(III) and Eu(III), it is too low for efficient sensitization of Pr(III).

Next, a comparison can be made between the two Nd-MOFs **2** and **5** (Figure 12a,b). Whereas the emission spectra are rather similar (apart from a slightly higher noise level in part a), the excitation spectra differ in the sense that the transition labeled "a" cannot be seen in the case of **5**, but can be seen in the case of **2**. Instead, the broad band at short wavelengths seems to be slightly broader (or at least, shifted to longer wavelength and thus lower energies) in Figure 12b than in part a. If one assumes that this high-energy broad band in the excitation spectra originates from ligand (linker) absorption (singlet $S_0$ to excited singlet $S_1$), this would mean that the excited singlet level $S_1$ is at slightly lower energy in **5** than in **2**. This could be an indication that also the triplet level $T_1$ of the 2,5-$PDC^{2-}$ linker is located at slightly lower energy than that of the 1,4-$BDC^{2-}$ linker, although this is not necessarily the case. We have not been able to find or determine a value for the 2,5-$PDC^{2-}$ triplet energy level, but it is probably a safe assumption that substituting a carbon atom for a nitrogen atom in the phenyl ring of the linker would not have a very dramatic effect on the triplet energy level of the resulting molecules.

Further, one can have a look at one specific transition in the emission spectrum of **4** in Figure 14: the peak(s) labeled "h", corresponding to the $^5D_0 \rightarrow {}^7F_0$ transition in the Eu(III) ion. This is a transition between two energy levels that are both nondegenerate. This means that if one unique crystal site is present in the Eu(III)-containing material, this transition should be responsible for one peak only. Crystal field effects cannot split this peak into more subpeaks. This also means that when more than one peak is encountered for this transition, it points to more than one crystallographic Eu(III) site being present in the material. Close inspection of transition "h" reveals two separate peaks, which indeed corresponds to what is seen in the crystal structure (Figures 1 and 2): two crystallographically different Eu(III) ions exist in compound **4**.

Finally, Table 3 lists the luminescence decay times that have been recorded for compounds **1**−**5**. The decay traces can be found in the Supporting Information (Figures S4−S7). All decay curves could be fitted with a single exponential. For compound **4**, this seems to contradict the fact that the two Eu(III) ions present in the crystal structure have a (slightly) different coordination environment, leading to the observation of two peaks for the $^5D_0 \rightarrow {}^7F_0$ transition. In principle, when the two crystallographic environments would be sufficiently different, it is assumed that each Eu(III) ion would have its own decay profile, leading to the necessity of (at least) two exponential terms to fit the decay curve. However, it is not unusual to have two (slightly) different sites with closely related time-dependent luminescence behavior, resulting in a single exponential term being able to fit the overall decay curve.

**Table 3. Luminescence Decay Times $\tau$ for Compounds 1−5**

| compd | $Ln^{3+}$ ion | linker | $\tau/\mu s$ |
|---|---|---|---|
| 1 | $Pr^{3+}$ | 1,4-$BDC^{2-}$ | 11 |
| 2 | $Nd^{3+}$ | 1,4-$BDC^{2-}$ | 0.43 |
| 3 | $Sm^{3+}$ | 1,4-$BDC^{2-}$ | 11 |
| 4 | $Eu^{3+}$ | 1,4-$BDC^{2-}$ | 475 |
| 5 | $Nd^{3+}$ | 2,5-$PDC^{2-}$ | 0.32 |

The values of the observed decay times can be compared with values obtained for other lanthanide complexes and MOFs; e.g., Bassett et al. find 0.46 ms for a Eu-containing bis-diketone complex, allbeit in a DMF matrix at 77 K (compared with our value of 0.475 ms for compound **4**).[45] In the same paper, a value of 13 $\mu$s was found for the homologous Sm-complex in DMF (as compared to 11 $\mu$s for our compound **3**), and a value of 1.5 $\mu$s was found for the Nd-homologue in deuterated DMF. We have published values for decay times of Nd-quinolinate complexes in the order of 0.5 $\mu$s, which also correspond to the values reported here (0.43 $\mu$s for **2** and 0.32 $\mu$s for **5**).[46] Finding luminescence decay times for a praseodymium-based coordination compound turns out not to be very easy, as most decay times have been reported for Pr-doped crystals and glasses. However, Voloshin et al. have stated that the decay time of a series of Pr-chelates (betadiketonates and carboxylates) in solution was shorter than the 4 $\mu$s


dx.doi.org/10.1021/ic301544q | Inorg. Chem. 2012, 51, 11623−11634

detection limit of their setup.[47] Mahlik et al. reported decay times between 23 and 6.5 $\mu$s as a function of pressure in a $Gd_3Ga_5O_{12}:Pr^{3+}$ crystal.[48] In that respect, our value of 11 $\mu$s for compound **1** compares well with the reported literature values.

The best way to compare the luminescence efficiency of the coordination polymers reported in this work with other MOFs that have been reported is to compare the quantum yields $Q$ (other symbols that are being used for quantum yield are $\Phi$ or $\eta$). Theoretically, the quantum yield is defined as the ratio of the amount of emitted photons to the amount of absorbed photons. When a rare-earth ion is directly excited in one of its $^{2S+1}L_J$ energy levels, this quantum yield can also be written as the ratio between the observed luminescence decay time $\tau$ and the radiative "natural" decay time $\tau_R$ of that specific lanthanide ion.

An excellent literature source on luminescent lanthanide-containing MOFs is the very recent review by Cui et al.[39] In this review, an overview is given of luminescent MOFs, among which is the specific class of luminescent lanthanide MOFs. However, when looking through the references given in this review, it is clear that very few papers mention the quantum yield of the observed luminescence. A little more common (but still rather rare) is the mentioning of the observed luminescence decay time $\tau$. Most papers only report a steady state emission spectrum, from which it is impossible to compare intensities in a reliable way. As a result, we have looked for published luminescence decay time values, in order to compare these with the values obtained for our materials. (Strictly speaking, for a lanthanide complex in which the ligands are used to harvest the excitation light, one has to take into account also the efficiency of the intersystem crossing (from the ligand excited singlet state $S_1$ to excited triplet state $T_1$), as well as the efficiency of the triplet $T_1$ to Ln excited state energy transfer). However, as a crude approximation, one can state that the longer the observed luminescence decay time is, the more efficient the luminescent material is.

In Cui's review, no praseodymium MOFs have been included, as the first one was only reported a few months ago. However, this paper did not mention a luminescence decay time. As such, we cannot compare the efficiency of our praseodymium MOF **1** with other luminescent praseodymium MOFs. The review contains six references to luminescent neodymium MOFs. However, also here, none contains a quantum yield or a luminescence decay time. As such, we cannot compare the efficiency of our neodymium MOFs **2** and **5** with others. The review contains only three references to luminescent samarium MOFs, but none reports a quantum yield or a decay time, so comparison of our luminescent samarium MOF **3** is not possible either. Predictably, the review contains many (25 to be exact) references to luminescent europium MOFs, as these have been most widely studied. Nine of these references contain luminescent decay times, ranging from 0.344 ms to above 2 ms. Of these nine references, three deal with terephthalate linkers, just as in our europium MOF **4**. The reported luminescence decay times range between 0.344 and 0.47 ms (hydrated europium terephthalate MOFs) to 0.94 ms (anhydrous europium terephthalate MOF). Thus, the decay time value of 0.475 ms for our (hydrated) europium terephthalate MOF **4** compares very well with earlier reported literature values.

## CONCLUSION

In conclusion, we have reported a hitherto unknown crystal structure from a europium terephthalate MOF and three isostructural rare-earth MOFs containing the light lanthanides praseodymium, neodymium, and samarium. This new crystal structure is most likely a consequence of the larger ionic radius of these light lanthanide ions, rather than of the slightly altered synthesis procedure that was followed. Rietveld refinement was used to prove that the powder XRD pattern at low $2\theta$ values is entirely dominated by the heavy elements, and as such, evidence was gathered that the praseodymium, neodymium, and samarium MOFs based on the terephthalate linker are isostructural with the reported crystal structure of the europium terephthalate MOF.

Aside from the terephthalate-based MOFs described above, a 2,5-pyridinedicarboxylate-based neodymium MOF was also synthesized, which turned out to have an identical crystal structure to that of previously reported MOFs that had been synthesized following the same procedure.

An in-depth luminescence study showed that the terephthalate linker is not really a very good sensitizer of lanthanide luminescence (with possible exception of europium), but nevertheless, rare emission spectra of praseodymium and samarium MOFs have been collected. A comparison was made between the luminescence behavior of the terephthalate-based and the 2,5-pyridinedicarboxylate-based neodymium MOFs, but the observed near-infrared emission was weak in both cases.

## ASSOCIATED CONTENT

### Supporting Information

FT-IR spectra of compounds **1**−**5**; TGA trace of compound **4**; fitted luminescence decay curves of compounds **1**−**5**. This material is available free of charge via the Internet at http://pubs.acs.org.

CCDC-891471 and CCDC-891472 contain the supplementary crystallographic data for this paper and can be obtained free of charge via www.ccdc.cam.ac.uk/conts/retrieving.html (or from the Cambridge Crystallographic Data Centre, 12 Union Road, Cambridge CB2 1EZ, U.K., fax: +44-1223-336033 or e-mail deposit@ccdc.cam.ac.uk).

## AUTHOR INFORMATION

### Corresponding Author

*E-mail: rik.vandeun@ugent.be. Phone: +3292644420. Fax: +3292644983.

### Notes

The authors declare no competing financial interest.

## ACKNOWLEDGMENTS

R.V.D. thanks the Hercules Foundation (Project AUGE/09/024 "Advanced Luminescence Setup") and Ghent University (BOF Project 01N01010) for financial support. P.V.D.V. acknowledges Ghent University (GOA Grant 01G00710 and BAS Grant 01B00608). R.V.D. and P.V.D.V. thank the FWO-Flanders (Research Project G.0081.10N).

## REFERENCES

(1) Eddaoudi, M.; Kim, J.; Rosi, N.; Vodak, D.; Wachter, J.; O'Keeffe, M.; Yaghi, O. M. *Science* **2002**, *295*, 469−472.

(2) Rosi, N. L.; Eckert, J.; Eddaoudi, M.; Vodak, D. T.; Kim, J.; O'Keeffe, M.; Yaghi, O. M. *Science* **2003**, *300*, 1127−1129.

(3) Ockwig, N. W.; Delgado-Friedrichs, O.; O'Keeffe, M.; Yaghi, O. M. *Acc. Chem. Res.* **2005**, *38*, 176−182.
(4) Li, J. R.; Kuppler, R. J.; Zhou, H. C. *Chem. Soc. Rev.* **2009**, *38*, 1477−1504.
(5) Chae, H. K.; Siberio-Perez, D. Y.; Kim, J.; Go, Y.; Eddaoudi, M.; Matzger, A. J.; O'Keeffe, M.; Yaghi, O. M. *Nature* **2004**, *427*, 523−527.
(6) Lee, J.; Farha, O. K.; Roberts, J.; Scheidt, K. A.; Nguyen, S. T.; Hupp, J. T. *Chem. Soc. Rev.* **2009**, *38*, 1450−1459.
(7) Ferey, G. *Chem. Soc. Rev.* **2008**, *37*, 191−214.
(8) Hong, D. Y.; Hwang, Y. K.; Serre, C.; Ferey, G.; Chang, J. S. *Adv. Funct. Mater.* **2009**, *19*, 1537−1552.
(9) Llewellyn, P. L.; Maurin, G.; Devic, T.; Loera-Serna, S.; Rosenbach, N.; Serre, C.; Bourrelly, S.; Horcajada, P.; Filinchuk, Y.; Ferey, G. *J. Am. Chem. Soc.* **2008**, *130*, 12808−12814.
(10) Fang, Q. R.; Zhu, G. S.; Xue, M.; Zhang, Q. L.; Sun, J. Y.; Guo, X. D.; Qiu, S. L.; Xu, S. T.; Wang, P.; Wang, D. J.; Wei, Y. *Chem.—Eur. J.* **2006**, *12*, 3754−3758.
(11) Eddaoudi, M.; Moler, D. B.; Li, H. L.; Chen, B. L.; Reineke, T. M.; O'Keeffe, M.; Yaghi, O. M. *Acc. Chem. Res.* **2001**, *34*, 319−330.
(12) Tranchemontagne, D. J. L.; Ni, Z.; O'Keeffe, M.; Yaghi, O. M. *Angew. Chem., Int. Ed.* **2008**, *47*, 5136−5147.
(13) Tranchemontagne, D. J.; Mendoza-Cortes, J. L.; O'Keeffe, M.; Yaghi, O. M. *Chem. Soc. Rev.* **2009**, *38*, 1257−1283.
(14) Champness, N. R. *Dalton Trans.* **2006**, 877−880.
(15) Reineke, T. M.; Eddaoudi, M.; Fehr, M.; Kelley, D.; Yaghi, O. M. *J. Am. Chem. Soc.* **1999**, *121*, 1651−1657.
(16) Reineke, T. M.; Eddaoudi, M.; O'Keeffe, M.; Yaghi, O. M. *Angew. Chem., Int. Ed.* **1999**, *38*, 2590−2594.
(17) White, K. A.; Chengelis, D. A.; Gogick, K. A.; Stehman, J.; Rosi, N. L.; Petoud, S. *J. Am. Chem. Soc.* **2009**, *131*, 18069−18070.
(18) *CrysAlis PRO, Version 1.171.34.34*; Agilent Technologies UK Ltd.: Yarnton, U.K., 2010.
(19) Sheldrick, G. M. *Acta Crystallogr.* **2008**, *A64*, 112−122.
(20) *SHELXTL-NT, Manual Version 5.1*; Bruker Analytical X-ray Systems Inc.: Madison, WI, 1997.
(21) Guo, X.; Zhu, G.; Sun, F.; Li, Z.; Zhao, X.; Li, X.; Wang, H.; Qiu, S. *Inorg. Chem.* **2006**, *45*, 2581−2587.
(22) Na, L.; Hua, R.; Zhang, L.; Zhang, W.; Ning, G. *J. Chem. Crystallogr.* **2009**, *39*, 688−691.
(23) Huang, Y.; Song, Y.-S.; Yan, B.; Shao, M. *J. Solid State Chem.* **2008**, *181*, 1731−1737.
(24) Qin, C.; Wang, X.-L.; Wang, E.-B; Su, Z.-M. *Inorg. Chem.* **2005**, *44*, 7122−7129.
(25) Allen, F. H. *Acta Crystallogr.* **2002**, *B58*, 380−388.
(26) Macrae, C. F.; Bruno, I. J.; Chisholm, J. A.; Edgington, P. R.; McCabe, P.; Pidcock, E.; Rodriguez-Monge, L.; Taylor, R.; van de Streek, J.; Wood, P. A. *J. Appl. Crystallogr.* **2008**, *41*, 466−470.
(27) Zhang, Z.-H.; Wan, S.-Y.; Okamura, T.; Sun, W.-Y.; Ueyama, N. *Z. Anorg. Allg. Chem.* **2006**, *632*, 679−683.
(28) Zhang, W.-Z. *Acta Crystallogr.* **2006**, *E62*, m1600−m1602.
(29) Chen, B.; Yang, Y.; Zapata, F.; Qian, G.; Luo, Y.; Zhang, J.; Lobkovsky, E. B. *Inorg. Chem.* **2006**, *45*, 8882−8886.
(30) He, H.; Yuan, D.; Ma, H.; Sun, D.; Zhang, G.; Zhou, H.-C. *Inorg. Chem.* **2010**, *49*, 7605−7607.
(31) Zhang, Y.; Yang, J.; Li, G.-D.; Zhang, F.; Chen, J.-S. *J. Coord. Chem.* **2008**, *61*, 945−955.
(32) Han, Y.; Li, X.; Li, L.; Ma, C.; Shen, Z.; Song, Y.; You, X. *Inorg. Chem.* **2010**, *49*, 10781−10787.
(33) Zhang, G.; Wang, Q.; Qian, Y.; Yan, G.; Ma, J. S. *J. Mol. Struct.* **2006**, *796*, 187−194.
(34) Shannon, R. D. *Acta Crystallogr.* **1976**, *A32*, 751−767.
(35) Bünzli, J. C. G.; Piguet, C. *Chem. Soc. Rev.* **2005**, *34*, 1048−1077.
(36) Bünzli, J. C. G.; Piguet, C. *Chem. Rev.* **2002**, *102*, 1897−1928.
(37) Bünzli, J. C. G. *Acc. Chem. Res.* **2006**, *39*, 53−61.
(38) Allendorf, M. D.; Bauer, C. A.; Bhakta, R. K.; Houk, R. J. T. *Chem. Soc. Rev.* **2009**, *38*, 1330−1352.
(39) Cui, Y. L.; Yue, Y. F.; Qian, G. D.; Chen, B. L. *Chem. Rev.* **2012**, *112*, 1126−1162 and references therein.
(40) An, J. Y.; Shade, C. M.; Chengelis-Czegan, D. A.; Petoud, S.; Rosi, N. L. *J. Am. Chem. Soc.* **2011**, *133*, 1220−1223.
(41) Görller-Walrand, C.; Binnemans, K. Rationalization of Crystal-Field Parametrization. In *Handbook on the Physics and Chemistry of Rare Earths*; Gschneidner, K. A., Jr., Eyring, L., Eds.; Elsevier Science: Amsterdam, 1996; Vol. *23*, Chapter 155, pp 121−284.
(42) Görller-Walrand, C.; Binnemans, K. Spectral Intensities of f-f Transitions. In *Handbook on the Physics and Chemistry of Rare Earths*; Gschneidner, K. A., Jr., Eyring, L., Eds.; Elsevier Science: Amsterdam, 1998; Vol. *25*, Chapter 167, pp 101−264.
(43) Feng, X.; Wang, Y.-F.; Shi, Z.-Q.; Shang, J.-J.; Wang, L.-Y. *Inorg. Chem. Commun.* **2012**, *22*, 131−136.
(44) Hilder, M.; Junk, P. C.; Kynast, U. H.; Lezhnina, M. M. *J. Photochem. Photobiol., A* **2009**, *202*, 10−20.
(45) Bassett, A. P.; Magennis, S. W.; Glover, P. B.; Lewis, D. J.; Spencer, N.; Parsons, S.; Williams, R. M.; De Cola, L.; Pikramenou, Z. *J. Am. Chem. Soc.* **2004**, *126*, 9413−9424.
(46) Van Deun, R.; Fias, P.; Nockemann, P.; Van Hecke, K.; Van Meervelt, L.; Binnemans, K. *Eur. J. Inorg. Chem.* **2007**, 302−305.
(47) Voloshin, A. I.; Shavaleev, N. M.; Kazakov, V. P. *J. Lumin.* **2001**, *93*, 199−204.
(48) Mahlik, S.; Malinowski, M.; Grinberg, M. *Opt. Mater.* **2011**, *33*, 1525−1529.
(49) Carnall, W. T.; Fields, P. R.; Rajnak, K. *J. Chem. Phys.* **1968**, *49*, 4424−4442.
(50) Carnall, W. T.; Fields, P. R.; Rajnak, K. *J. Chem. Phys.* **1968**, *49*, 4450−4455.